Supporting Information

Synergetic electronic modulation and nanostructure engineering of heterostructured RuO_2/Co_3O_4 as advanced bifunctional electrocatalyst for Zinc-air batteries

Xiaojie Zhuang,‡[a] Yitong Zhou,‡[a] Zhongqing Jiang,[b] Xianzhi Yao[c] and Xin-Yao Yu*[a,d]*

[a]*Institutes of Physical Science and Information Technology, Anhui University, Hefei 230601 (P. R. China). Email: yuxinyao@ahu.edu.cn.*

[b]*Key Laboratory of Optical Field Manipulation of Zhejiang Province, Department of Physics, Zhejiang Sci-Tech University, Hangzhou 310018 (P. R. China). Email: zhongqingjiang@zstu.edu.cn*

[c]*Ningbo Research Institute of Ecological and Environmental Sciences, Ningbo 315000 (P. R. China).*

[d]*School of Materials Science and Engineering, Anhui University, Hefei 230601 (P. R. China).*

‡These two authors contribute equally to this work.

*Corresponding authors

Experimental

Chemicals

Cobalt(III) nitrate hexahydrate [$Co(NO_3)_2 \cdot 6H_2O$, AR, 98.5%], glycerol ($C_3H_8O_3$, AR, 99.0%) and isopropyl alcohol (C_3H_8O, AR, 99.0%) were purchased from Sinopharm Chemical Reagent Co, Ltd (China). Ruthenium(III) chloride hydrate (Cl_3H_2ORu, AR, 98%) was obtained from Shanghai Maclin Biochemical Technology Co., Ltd. All the reagents were received without further refinement.

Synthesis of Co-gly SSs

The Co-gly SSs were first prepared through a one-pot solvothermal process. Typically, 0.38 mmol of $Co(NO_3)_2 \cdot 6H_2O$ was dissolved in a mixed solvent containing 8 ml of glycerol and 40 ml of isopropanol. After stirring for 20 min at room temperature, the homogeneous solution was transferred to a Teflon-lined stainless steel autoclave and subsequently treated at 180 ^oC for 6 h. When the temperature was cooled down naturally, the resulting solution was centrifuged and the collected products were washed with absolute ethyl alcohol for three times and then dried at 60 ^oC overnight.

Synthesis of RuCo-pre HSs

To obtain the RuCo-pre HSs, 60 mg of dried Co-gly SSs were first dispersed in 40 ml of deionized water by ultrasonic treatment. Then, 15 mg of $RuCl_3 \cdot xH_2O$ was added into the above solution and stirred for 6 h at room temperature. Finally, Ru-Co RuCo-pre HSs were collected by centrifuging and washed with DIW for three times before drying at 60 ^oC overnight. For comparison, the precursors were also synthesized with different addition of $RuCl_3 \cdot xH_2O$ (0, 10 and 20 mg), and the obtained products were named as Co-pre HSs, RuCo-pre-1 HSs, and RuCo-pre-2 HSs, respectively.

Synthesis of RuCoO HSs

The RuCoO HSs were obtained by annealing RuCo-pre HSs at 300 ^oC for 3 h under air atmosphere with a heating rate of 5 $^oC\ min^{-1}$. As control samples, the RuCo-pre HSs were calcined at different temperature of 200 ^oC and 400 ^oC and the obtained products were denoted as RuCoO-200 ^oC HSs and RuCoO-400 ^oC HSs, respectively. In addition, the metal oxides obtained by calcinating Co-pre HSs, RuCo-pre-1 HSs, and RuCo-pre-2 HSs are named as Co_3O_4 HSs, RuCoO-1 HSs, and RuCoO-2 HSs, respectively.

Materials characterization

The X-ray diffraction (XRD) patterns were collected by a Bruker AXS GmbH diffractometer in the 2θ range of 5-80^o. The morphology and structure of the materials were characterized using scanning electron microscopy (SEM) on Regulus 8230 scanning electron microscope. Transmission electron microscopy (TEM) and high-resolution TEM (HRTEM) images were collected on JEM-2100F. Nicolet iS50 spectrometer was employed to obtain the FTIR spectra. The N_2 adsorption-desorption measurements were carried out on Autosorb IQ-MP-MP. The Raman spectra were recorded on inVia-Reflex. The chemical valence of elements were studied using ESCALAB 250Xi instrument. The energy dispersive spectroscopy (EDS) mappings and selected area electron diffraction (SAED) patterns were obtained on JEOL-JEM 2100F.

Electrochemical measurements

The OER and ORR performance were evaluated on rotating ring-disk electrode using CHI 760E electrochemical workstation with a three-electrode system in 0.1 M KOH electrolyte. The Hg/HgO electrode, glassy carbon electrode (GCE) coated with catalysts, and carbon rod were used as reference electrode, working electrode, and counter electrode, respectively. Besides, all the measured potentials were transformed into reversible hydrogen electrode (RHE) using the following equation:

$$E_{(\text{V } vs.\ \text{RHE})} = E_{(\text{V } vs.\ \text{Hg/HgO})} + 0.0591 \times \text{pH} + 0.098$$

The working electrode was prepared as follows: 5 mg of as-synthesized electrocatalyst was uniformly dispersed in a mix solution containing 270 μL of ethyl alcohol, 200 μL of deionized water, and 30 μL of Nafion solution. Then, 2.5 μL of the homogeneous electrocatalyst ink was dropped onto the GCE (0.07 cm^2). For both ORR and OER test, the scan rates of cyclic voltammetry (CV) and linear sweep voltammetry (LSV) are 50 and 5 mV s^{-1}, respectively. The transferred electron numbers of ORR is calculated by the *K-L* equation provided as follows:

$$1/J = 1/J_K + 1/(B\omega^{1/2})$$

where J is the measured current density, J_K is the kinetic limiting current density, and ω is the rotating rate. B can be calculated from the Levich slope below:

$$B = 0.2nFC_0D_0^{2/3}v^{-1/6}$$

In this equation, n is the transferred electron numbers, F is Faraday constant (F = 96485 C mol^{-1}), and C_0 is the concentration of O_2 in the solution ($C_0 = 1.2 \times 10^{-6}$ mol cm^{-3}). D_0 is the diffusion coefficient of O_2 in 0.1 M KOH ($D_0 = 1.9 \times 10^{-5}$ cm^2 s^{-1}) and v is the kinematics viscosity of the electrolyte (v = 0.01 cm^2 s^{-1}). The double-layer capacitance (C_{dl}) was figured out by measuring CV curves at different scanning rates from 800 to 2400 rpm. The electrochemical impedance spectroscopy (EIS) was investigated under open circuit potential with a frequency range from 10^{-2} Hz to 10^5 Hz.

Zn-air batteries measurements

The aqueous rechargeable Zn-air battery is made up with carbon paper supported RuO_2/Co_3O_4 as air cathode and polished zinc foil as anode, and the electrolyte is 6.0 M KOH + 0.2 M $Zn(CH_3COO)_2$. The working electrode was prepared as follows: 20 mg of RuO_2/Co_3O_4 was firstly dispersed in a mixed solution containing 652 μL of isopropanol, 261 μL of deionized water, and 87 μL of Nafion solution. Then, 50 μl of the homogeneous electrocatalyst ink was dropped onto the carbon paper. As for flexible solid-state Zn-air battery, the gel electrolyte was prepared by following steps. First, 1 g of polyvinyl alcohol (PVA) was dissolved in 10 ml DIW and heated at 90 °C for 1 h. After that, 1 mL of mixed solution of 18 M KOH and 0.2 M $Zn(CH_3COO)_2$ is added and kept at 90 °C for another 1 h. In the end, the above solution was frozen for 2 h and recovered to room temperature naturally.

Computational methods

Spin-polarized DFT calculations were performed using the Vienna ab initio simulation package (VASP).[1,2] The generalized gradient approximation proposed by Perdew, Burke, and Ernzerhof (GGA-PBE) was selected for the exchange-correlation potential.[3] The pseudo-potential was described by the projector-augmented-wave (PAW) method.[4] The geometry optimization was performed until the Hellmann–Feynman force on each atom was smaller than 0.04 eV $Å^{-1}$. The energy criterion was set to 10^{-6} eV in iterative solution of the Kohn-Sham equation. The heterostructure was built by employing a

2*4 supercell of RuO_2 (110) and a 3*1 supercell of Co_3O_4 (110). The RuO_2 (110) part of the heterostructure contains 6 atomic layers and the Co_3O_4 (110) part is consisted of 4 atomic layers. Besides, adsorption studies were carried out after full optimization of heterostructure. Only 3 atomic layers of RuO_2 were allowed to move for adsorption studies on RuO_2 side, while it was 2 atomic layers of Co_3O_4 for adsorption on the other side. Additionally, the surfaces were both (110) for the investigation of pure Co_3O_4 and RuO_2. The vacuum above the surface was set to 12 Å. The free energy of O_2 was obtained from the reaction of $H_2 + 1/2O_2 = H_2O(l)$, where H_2 and H_2O were obained by DFT calculations. The adsorption energy was calculated according to $E_{adsorption} = E_{total} - E_{adsorbate} - E_{adsorbent}$, where E_{total}, $E_{adsorbate}$, and $E_{adsorbent}$ is the total DFT energy of adsorbed structure, DFT energy of adsorbate and DFT energy of adsorbent, respectively. Moreover, the overpotential of OER was determined by the maximum energy difference between two adjacent fundamental steps, while the overpotential of ORR was determined by the minimum energy difference between two adjacent elemental steps.

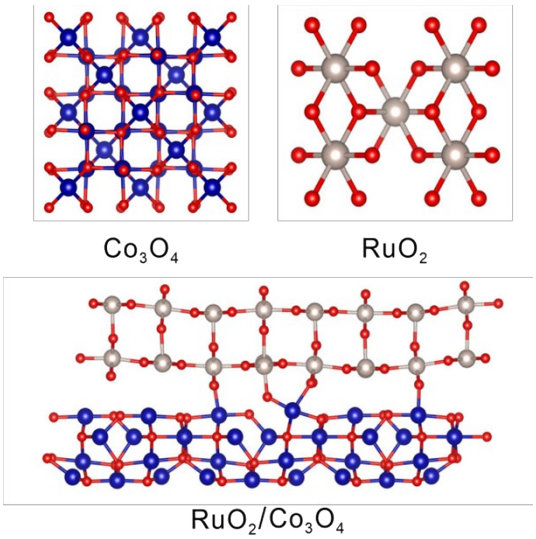

Fig. S1 Atomic models of Co_3O_4, RuO_2, and RuO_2/Co_3O_4. The blue, gray, and red balls represent Co, Ru, and O atoms, respectively.

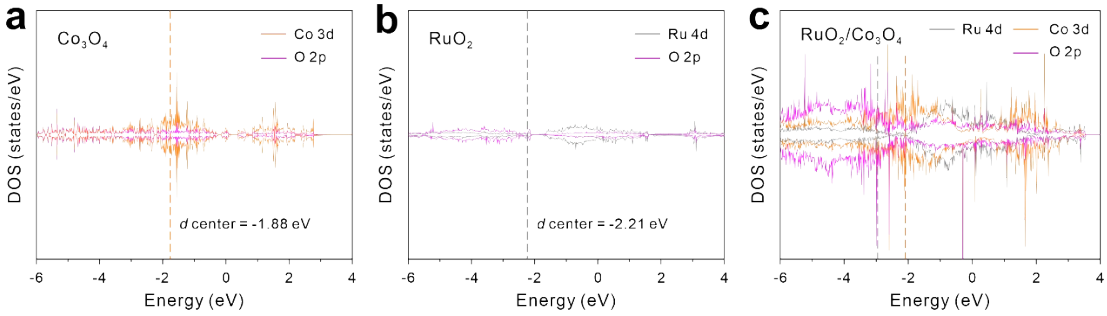

Fig. S2 PDOS of Co_3O_4 (a), RuO_2 (b), and RuO_2/Co_3O_4 (c).

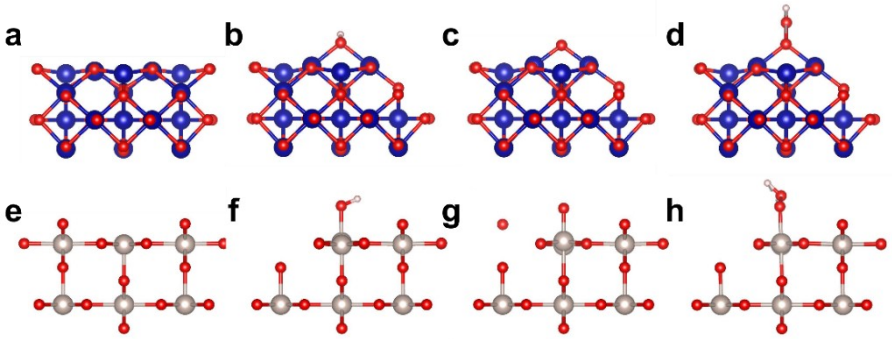

Fig. S3 (a,e) Atomic model of the (110) face of Co_3O_4 (a) and RuO_2 (e). (b-d) Adsorption configuration of OH* (b), O* (c), and OOH* (d) on Co_3O_4. (f-h) Adsorption configuration of OH* (f), O* (g), and OOH* (h) on RuO_2. The blue, gray, red, and white balls represent Co, Ru, O, and H atoms, respectively.

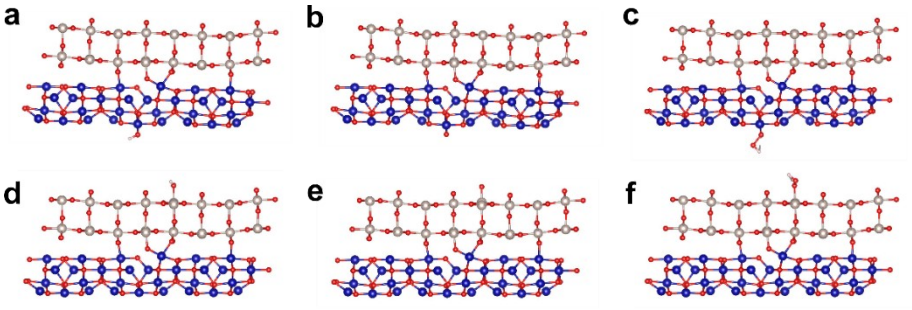

Fig. S4 (a-c) Adsorption configuration of OH* (a), O* (b), and OOH* (c) on the Co site of RuO_2/Co_3O_4. (d-f) Adsorption configuration of OH* (d), O* (f), and OOH* (g) on Ru site of RuO_2/Co_3O_4. The blue, gray, red, and white balls represent Co, Ru, O, and H atoms, respectively.

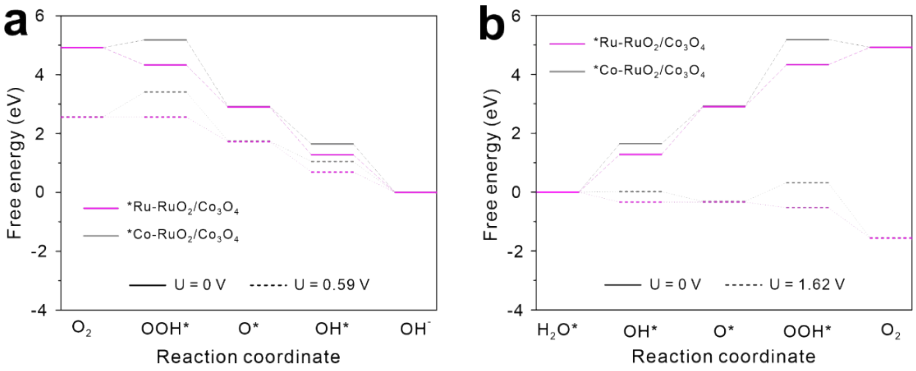

Fig. S5 Free energy diagrams at different applied potentials for (a) ORR and (b) OER.

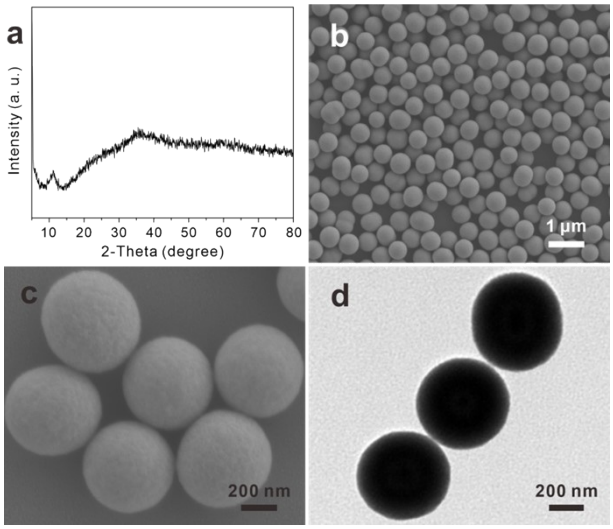

Fig. S6 (a) XRD pattern, (b,c) SEM images, and (d) TEM image of Co-gly SSs.

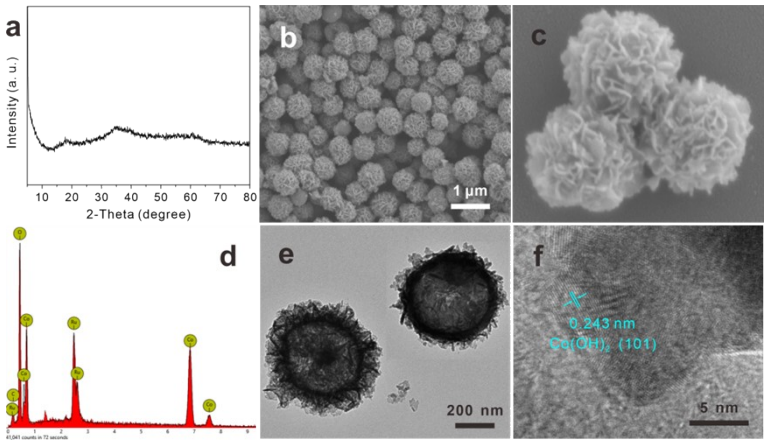

Fig. S7 (a) XRD pattern, (b,c) SEM images, (d) EDS spectra, (e) TEM image, and (f) HRTEM image of RuCo-pre HSs.

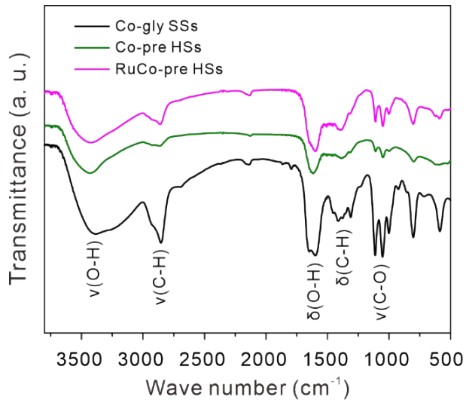

Fig. S8 FTIR spectrum of Co-gly SSs, Co-pre HSs, and RuCo-pre HSs. In the FTIR spectrum of Co-gly SSs, the broad absorption band at ~3400 cm^{-1} is assigned to hydrogen-bound hydroxyl group and the absorption band at ~2850 cm^{-1} is attributed to the C-H stretching vibration. The absorption bands lie in ~1650 and ~1350 cm^{-1} are indexed to O-H and C-H bending vibrations, respectively. Besides, the absorption band at ~1100 cm^{-1} is the characteristic of the C-O stretching vibration.[5] After reacting with water and $RuCl_3$, the metal-glycerate phase still exists in Co-pre and RuCo-pre HSs.

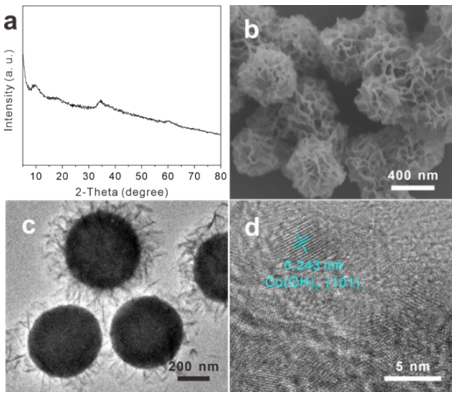

Fig. S9 (a) XRD pattern, (b) SEM image, (c) TEM image, and (d) HRTEM image of Co-pre HSs.

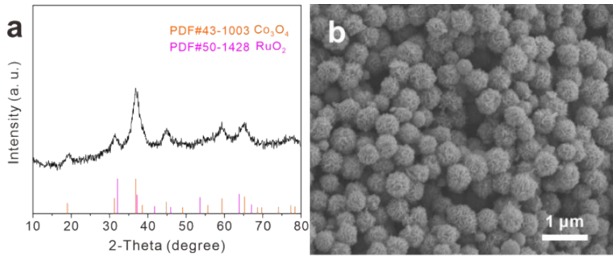

Element	Line Type	k factor	at%
O	K series	1.8686	48. 9
Co	K series	1.2611	46. 8
Ru	L series	1.7453	4. 3
Total:			100

Fig. S10 (a) XRD pattern, (b) SEM image, (c) STEM and corresponding elemental mapping images, and (d) EDS data of RuCoO HSs.

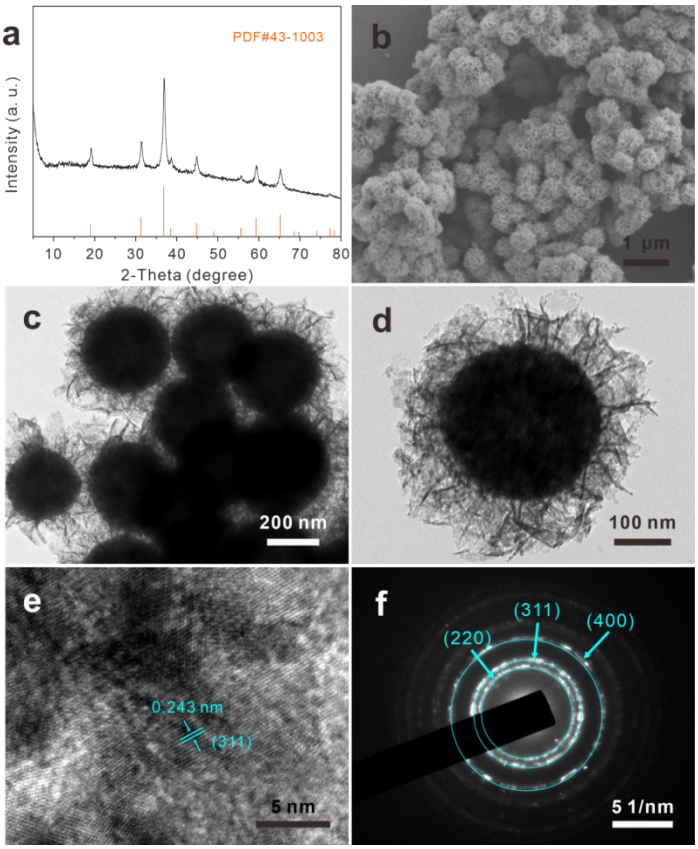

Fig. S11 (a) XRD pattern, (b) SEM image, (c,d) TEM images, (e) HRTEM image, and (f) SAED pattern of Co_3O_4 HSs.

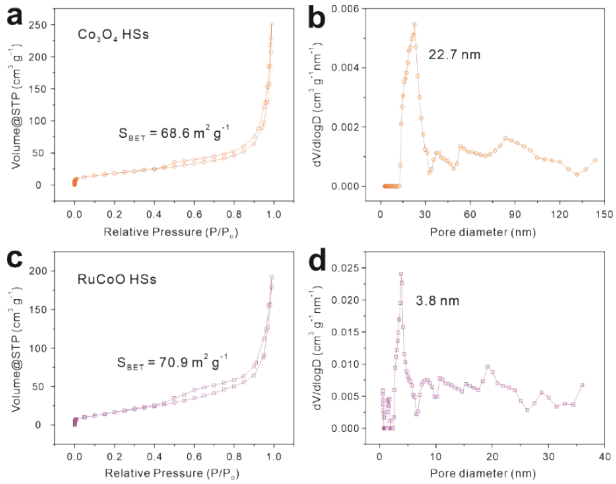

Fig. S12 N_2 adsorption/desorption isotherms and pore size distribution of Co_3O_4 HSs (a,b) and RuCoO HSs (c,d).

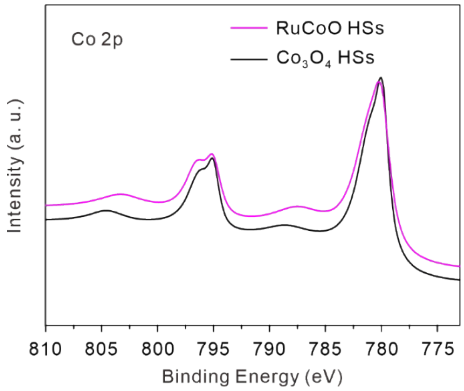

Fig. S13 Co 2p high-resolution XPS spectra of RuCoO and Co_3O_4 HSs.

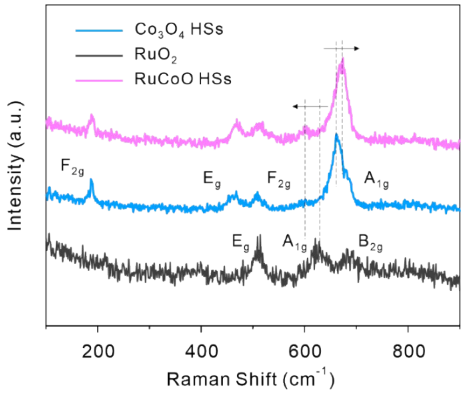

Fig. S14 Raman spectra of Co_3O_4 HSs, RuO_2, and RuCoO HSs.

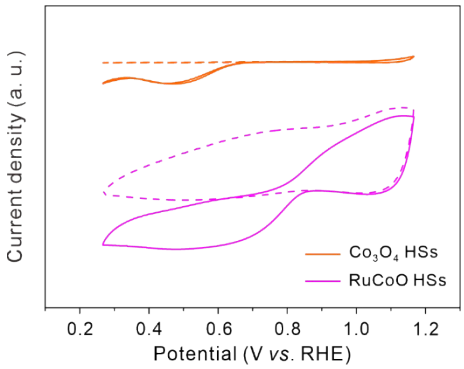

Fig. S15 CV curves of Co_3O_4 and RuCoO HSs tested in N_2-saturated (dash line) and O_2-saturated (solid line) 0.1 M KOH electrolyte.

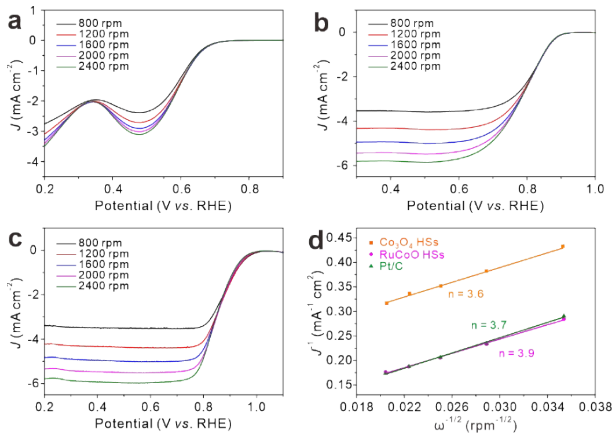

Fig. S16 LSV curves at different rotation rates from 800 to 2400 rpm in ORR region of (a) Co_3O_4 HSs, (b) RuCoO HSs, and (c) Pt/C. (d) K-L plots of Co_3O_4 HSs, RuCoO HSs, and Pt/C.

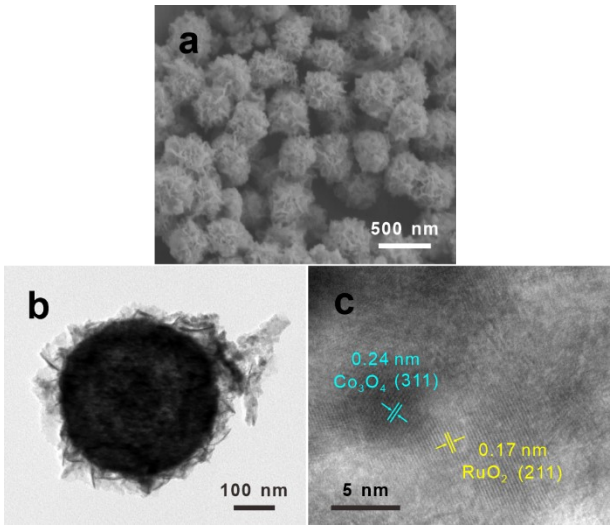

Fig. S17 (a) SEM image, (b) TEM image, and (c) HRTEM image of RuCoO HSs after ORR stability test.

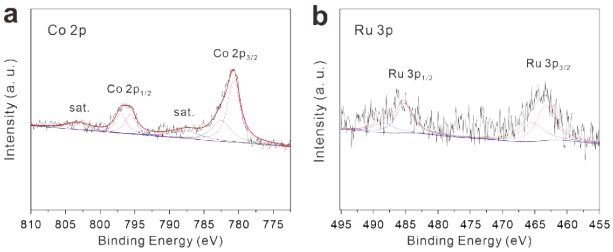

Fig. S18 (a) Co 2p and (b) Ru 3p high-resolution XPS spectra of RuCoO HSs after ORR stability test.

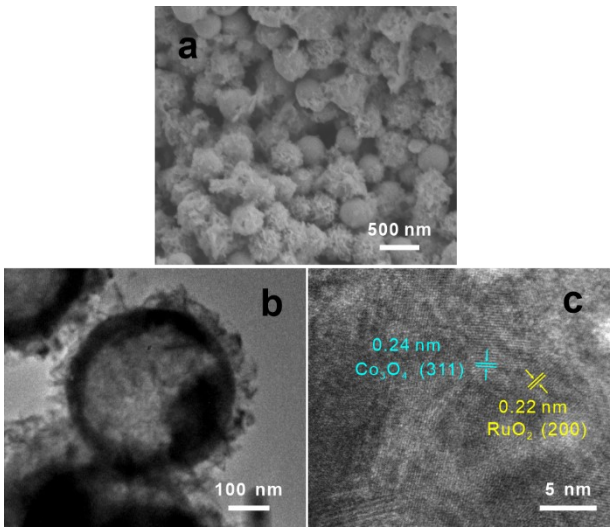

Fig. S19 (a) SEM image, (b) TEM image, and (c) HRTEM image of RuCoO HSs after OER stability test.

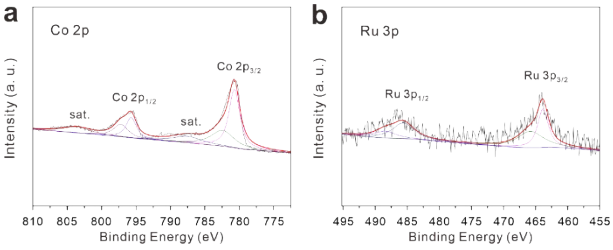

Fig. S20 (a) Co 2p and (b) Ru 3p high-resolution XPS spectra of RuCoO HSs after OER stability test.

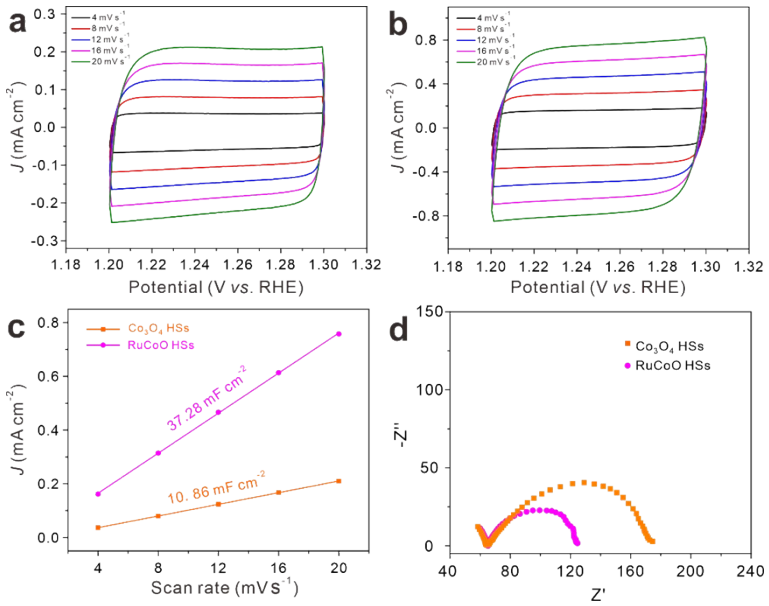

Fig. S21 CV curves at different scan rates from 4 to 20 mV s^{-1} of (a) Co_3O_4 HSs and (b) RuCoO HSs. (c) C_{dl} and (d) Nyquist plots of Co_3O_4 and RuCoO HSs.

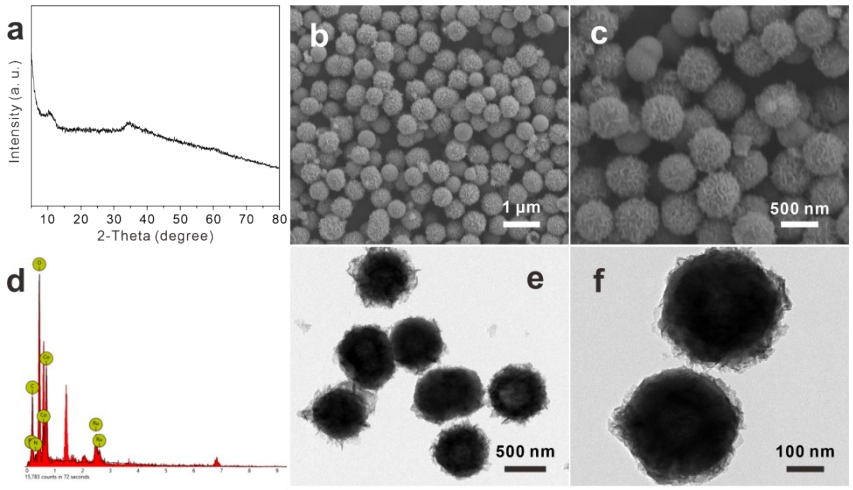

Fig. S22 (a) XRD pattern, (b,c) SEM images, (d) EDS spectra, and (e,f) TEM images of RuCo-pre-1 HSs.

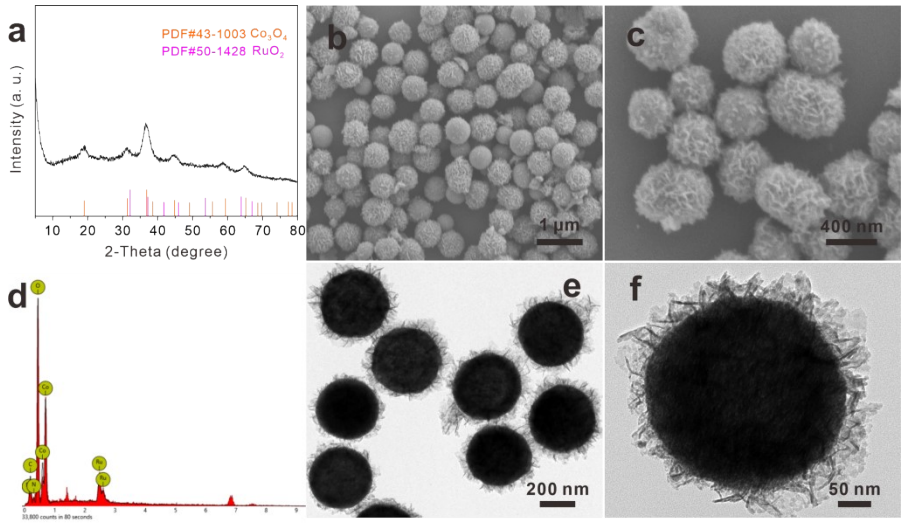

Fig. S23 (a) XRD pattern, (b,c) SEM images, (d) EDS spectra, and (e,f) TEM images of RuCoO-1 HSs.

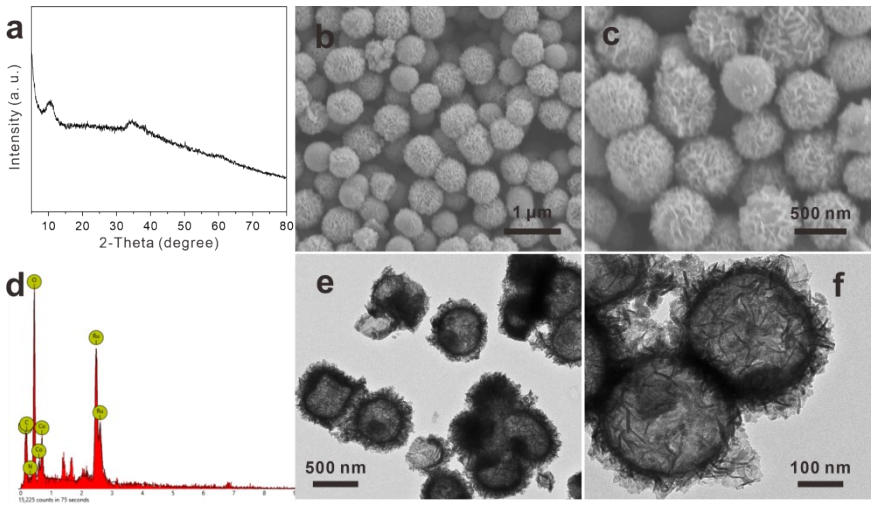

Fig. S24 (a) XRD pattern, (b,c) SEM images, (d) EDS spectra, and (e,f) TEM images of RuCo-pre-2 HSs.

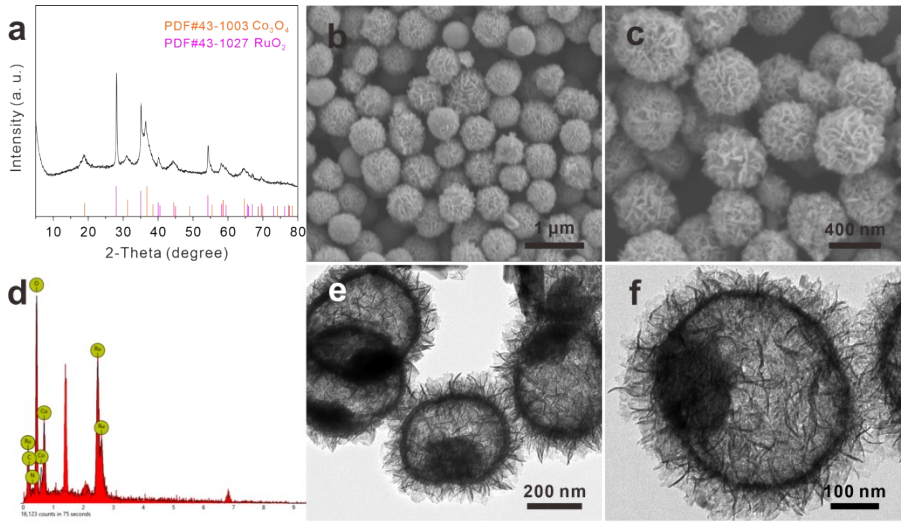

Fig. S25 (a) XRD pattern, (b,c) SEM images, (d) EDS spectra, and (e,f) TEM images of RuCoO-2 HSs.

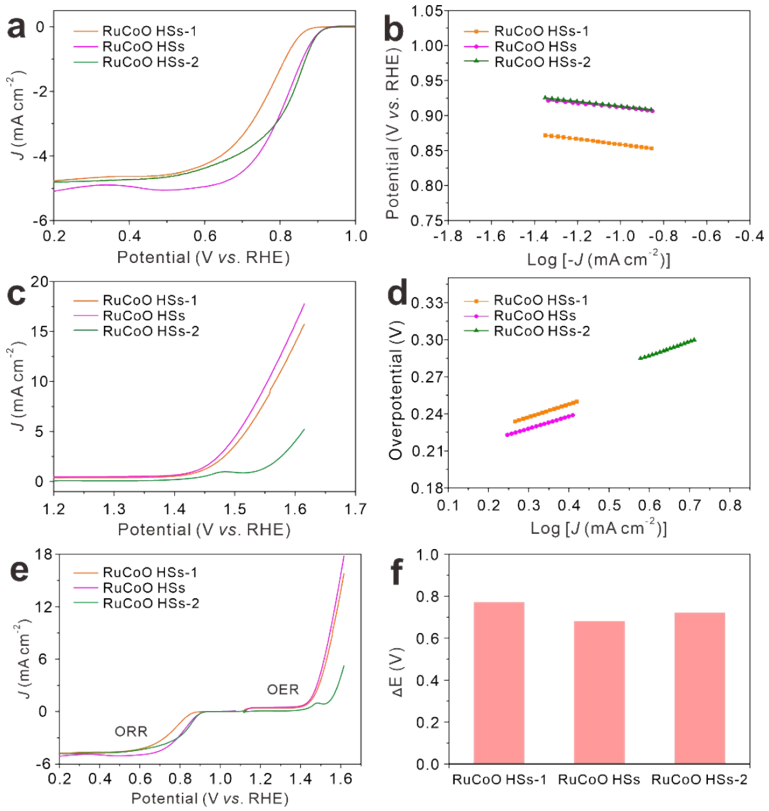

Fig. S26 Bifunctional performance of RuO_2/Co_3O_4 hollow spheres with different Ru loading. (a,c) LSV curves and (b,d) Tafel plots of ORR (a,c) and OER (b,d). (e) Overall LSV curves. (f) Value of potential gap.

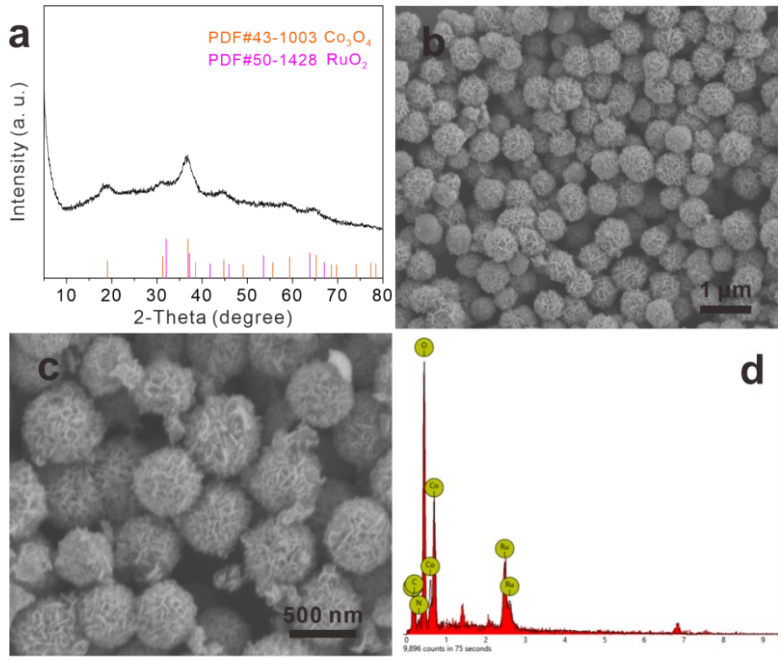

Fig. S27 (a) XRD pattern, (b,c) SEM images, and (d) EDS spectra of RuCoO-200 °C HSs.

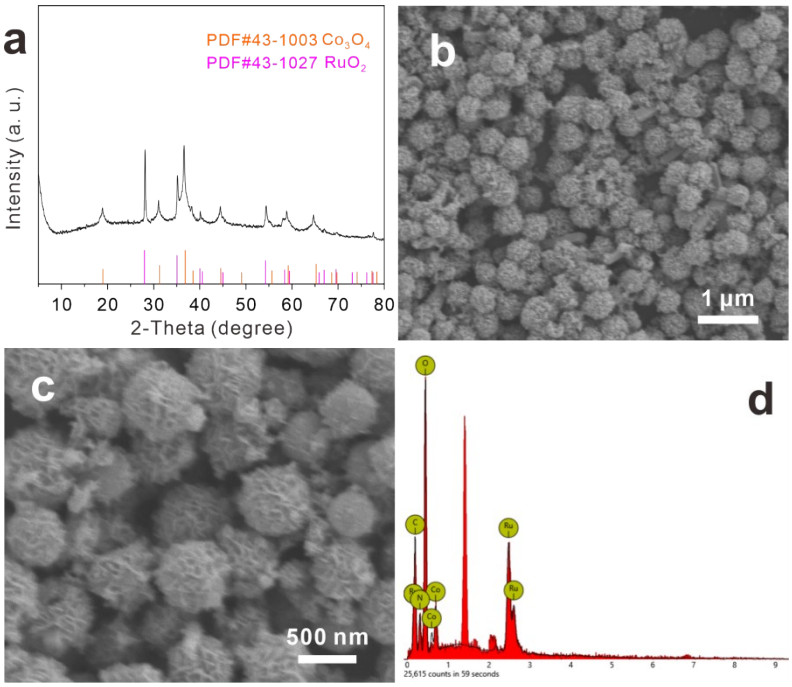

Fig. S28 (a) XRD pattern, (b,c) SEM images, and (d) EDS spectra of RuCoO-400 °C HSs.

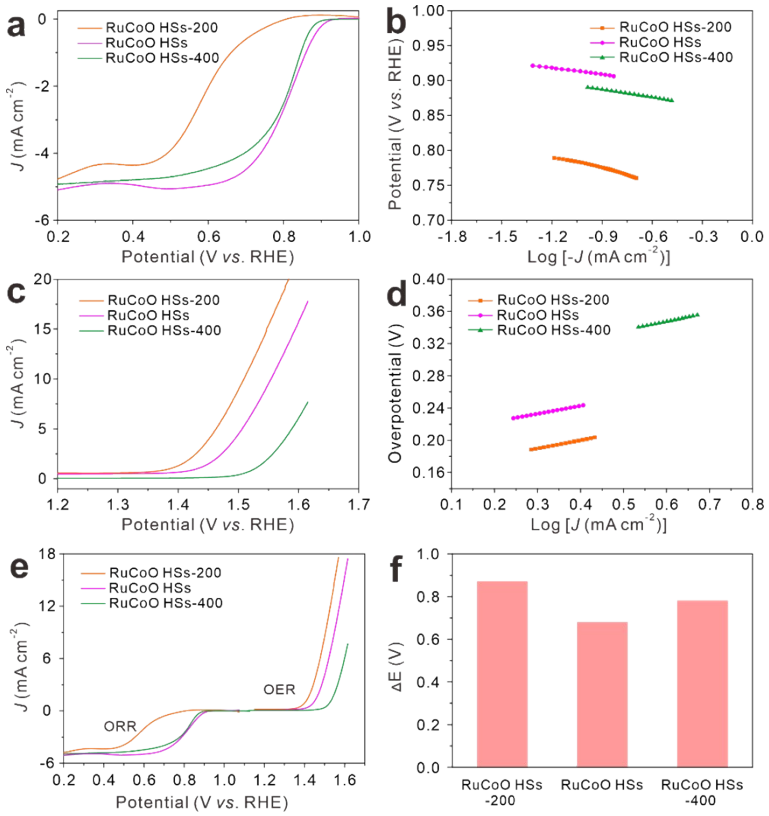

Fig. S29 Bifunctional performance of RuO_2/Co_3O_4 hollow spheres obtained at different calcination temperature. (a,c) LSV curves and (b,d) Tafel plots of ORR (a,c) and OER (b,d). (e) Overall LSV curves. (f) Value of potential gap.

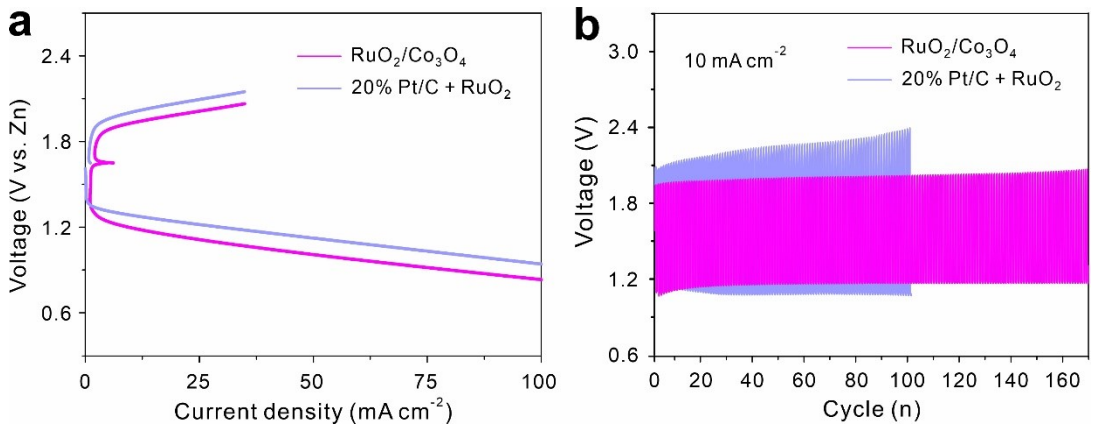

Fig. S30 (a) Charge/discharge polarization curves and (b) galvanostatic charge/discharge curves at 10 mA cm^{-2} of aqueous Zn-air battery.

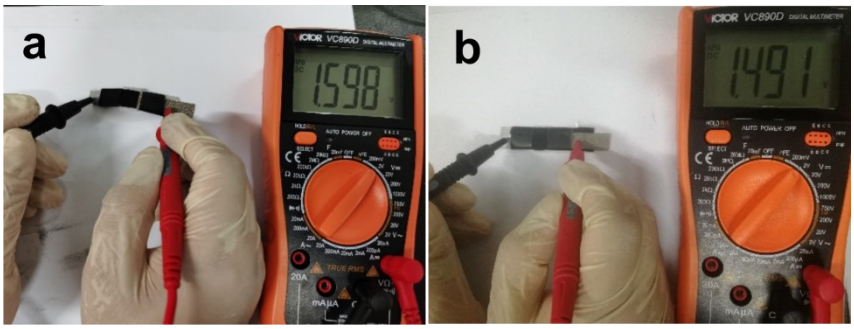

Fig. S31 Open-circuit voltage of flexible solid-state Zn-air battery with (a) RuCoO HSs and (b) Pt/C + RuO_2 as cathode electrocatalysts.

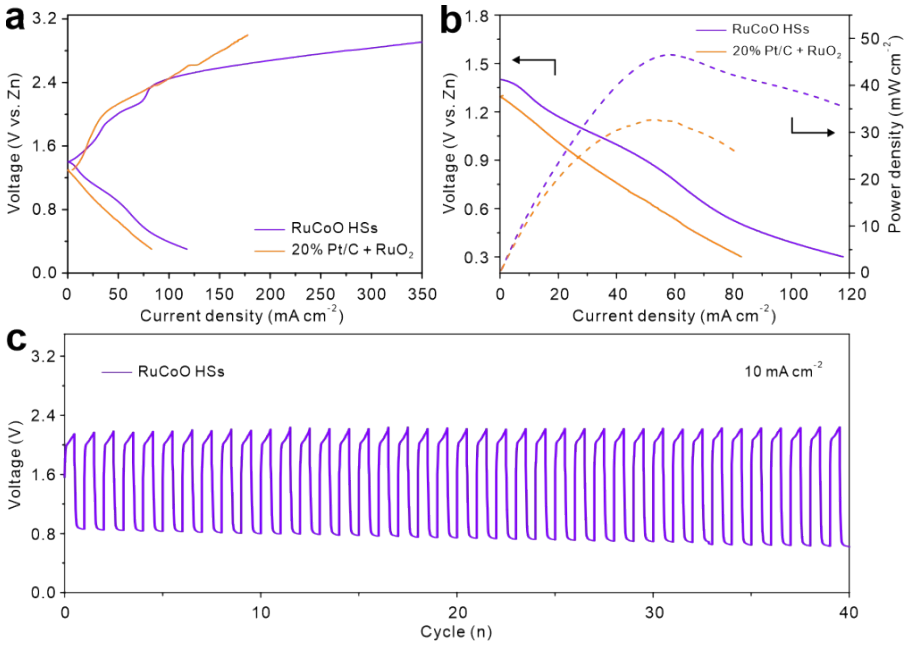

Fig. S32 (a) Charge/discharge polarization curves, (b) discharge polarization curves and the corresponding power density curves, and (c) galvanostatic charge/discharge curves at 10 mA cm^{-2} of flexible solid-state Zn-air battery.

Table S1 Performance comparison of the present rechargeable Zn-air batteries with other reported ones using liquid alkaline electrolytes.

Electrode material	Open circuit potential (V)	Power density (mW cm^{-2})	Cycling number	Energy efficiency (%)	Ref.
Al,P-codoped Co_3O_4 microspheres	1.43	89.1	150 cycles	61	6
Sulfur-doped $LaCoO_3$	1.47	92	300 cycles	52	7
Co_3O_4@3DMC	1.38	71	72 cycles	54.7	8
Co_3O_4 nanoplates	-	59.7	100 cycles	58	9
Fe/Co-N/P-9	1.38	-	145 cycles	51	10
Co_3O_4/ Co–N@NMC	1.46	122	108 cycles	42.8	11
N-Doped Porous Carbons	1.42	65	60 cycles	-	12
RuCoO HSs	**1.47**	**105**	**170 cycles**	**59**	**This work**

References

1 G. Kresse and J. Furthmüller, *Comp. Mater. Sci.*, 1996, **6**, 15.

2 Kresse, Furthmüller, *Phys. Rev. B*, 1996, **54**, 11169.

3 Perdew, Burke, Ernzerhof, *Phys. Rev. Lett.*, 1996, **77**, 3865.

4 Blöchl, *Phys. Rev. B*, 1994, **50**, 17953.

5 J. Zhao, Y. C. Zou, X. X. Zou, T. Y. Bai, Y. P. Liu, R. Q. Gao, D. J. Wang and G. D. Li, *Nanoscale*, 2014, **6**, 7255.

6 B. B. Guo, R. G. Ma, Z. C. Li, S. K. Guo, J. Luo, M. H. Yang, Q. Liu, T. J. Thomas and J. C. Wang, *Nano-Micro Lett.*, 2020, **12**, 20.

7 J. Ran, T. Wang, J. Zhang, Y. Liu, C. Xu, S. Xi, and D. Gao, *Chem. Mater.*, 2020, **32**, 3439-3446.
8 K. L. An, Y. Zheng, X. X. Xu and Y. Wang, *J. Solid State Chem.*, 2019, **270**, 539-546.
9 P. Tan, B. Chen, H. R. Xu, W. Z. Cai, W. He and M. Ni, *Energy*, 2019, **166**, 1241-1248.
10 J. Di, J. X. Guo, N. N. Wang and G. P. Ma, *ACS Sustainable Chem. Eng.*, 2019, **7**, 7716-7727.
11 Y. Q. Wang, X. X. Xu, L. Y. Liu, J. Chen and G. M. Shi, *Dalton Trans.*, 2019, **48**, 7150-7157.
12 X. W. Lv, Y. P. Liu, W. W. Tian, L. J. Gao and Z. Y. Yuan, *J. Energy Chem.*, 2020, **50**, 324-331.